Macromolecules

Article
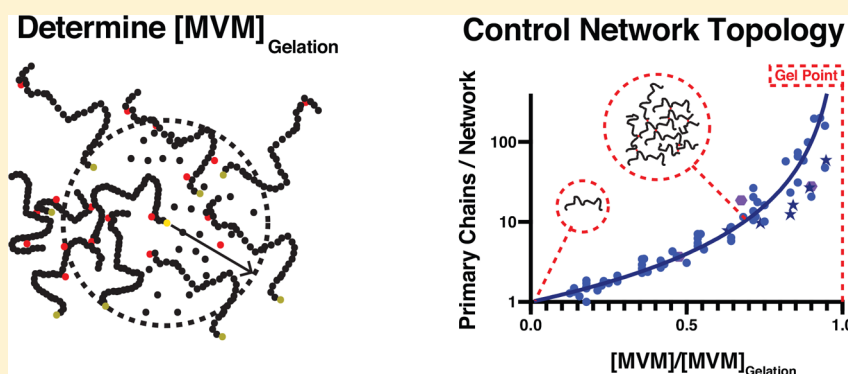
Universal Scaling Behavior during Network Formation in Controlled Radical Polymerizations

Joseph L. Mann, Rachel L. Rossi, Anton A. A. Smith, and Eric A. Appel*

Department of Materials Science and Engineering, Stanford University, Stanford, California 94305, United States

S Supporting Information

ABSTRACT: Despite the ubiquity of branched and network polymers in biological, electronic, and rheological applications, it remains difficult to predict the network structure arising from polymerization of vinyl and multivinyl monomers. While controlled radical polymerization (CRP) techniques afford modularity and control in the synthesis of (hyper)branched polymers, a unifying understanding of network formation providing grounded predictive power is still lacking. A current limitation is the inability to predict the number and weight average molecular weights that arise during the synthesis of (hyper)branched polymers using CRP. This study addresses this literature gap through first building intuition via a growth boundary analysis on how certain environmental cues (concentration, monomer choice, and cross-linker choice) affect the cross-link efficiency during network formation through experimental gel point measurements. We then demonstrate, through experimental gel point normalization, universal scaling behavior of molecular weights in the synthesis of branched polymers corroborated by previous literature experiments. Moreover, the normalization employed in this analysis reveals trends in the macroscopic mechanical properties of networks synthesized using CRP techniques. Gel point normalization employed in this analysis both enables a polymer chemist to target specific number and weight average molecular weights of (hyper)branched polymers using CRP and demonstrates the utility of CRP for gel synthesis.

INTRODUCTION

Beginning with Bakelite, Leo Baekeland's purely synthetic alternative to the exploding celluloid billiard balls of the late 19th century, the covalent junction of polymeric chains into synthetic networks has simultaneously puzzled polymer scientists and inspired a new generation of revolutionary materials with unprecedented material properties. Complete percolating networks, which have reached gelation, are the cornerstone of separation technologies[1−3] and afford tunable matrices for applications ranging from wearable electronics to soft contact lenses to cell culture.[4−6] Similarly, incomplete networks (i.e., soluble branched molecules or cyclized molecules) have been explored as platforms for nanomedicine,[7−12] diagnostic and imaging tools,[13−17] commodity plastic processing,[18−20] and viscosity modifiers.[21−24] Both incomplete and complete networks are also being explored as electrolytes for electronics.[25−29] The ubiquity and future potential of these materials are linked to the physical properties

afforded by a network and by the availability of modular handles to tune the network.

The molecular weight between cross-link junctions (M_x) is a key variable to determine network properties. M_x defines the pore size of complete networks, which in turn affects the diffusion coefficient of macromolecules and resulting mechanical properties.[30,31] This affords bespoke synthetic procedures to generate gels to separate or release different sized materials[32] or control cell morphology and differentiation.[33−35] In the case of insoluble, branched networks, M_x defines the degree of branching, which affects rheological and mechanical properties.[36,37] Moreover, in translational medicine, when incomplete networks are functionalized with bioactive molecules, the average number of primary chains per molecule and degree of branching afford functional handles to control
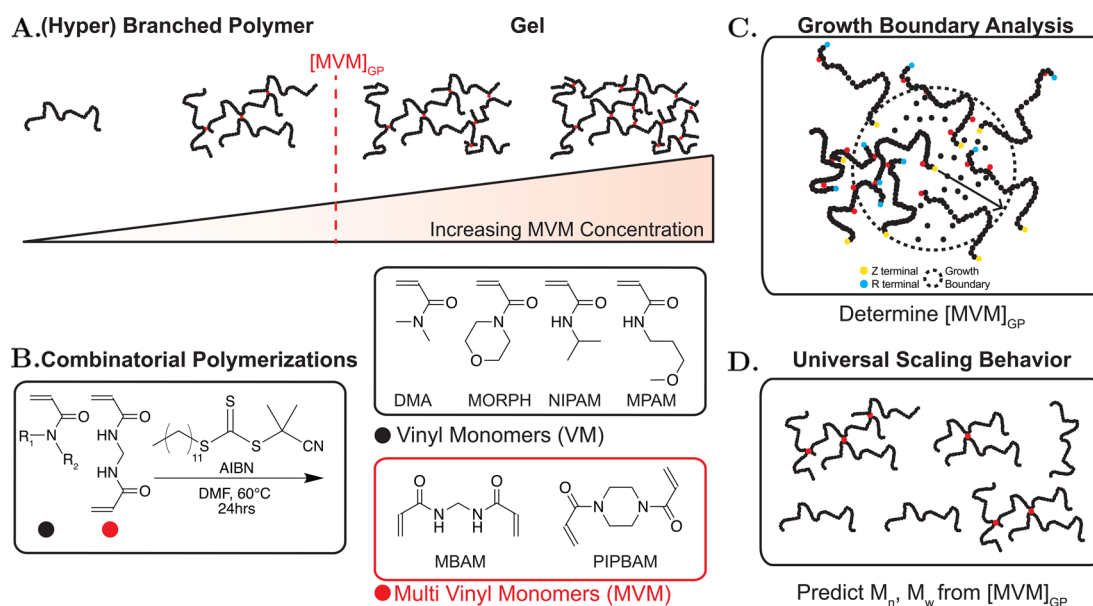
Figure 1. (A) Schematic of network formation with effective branch points (red dots) and primary chains (black chains) pre- and post-gelation. (B) Schematic of RAFT polymerization of vinyl monomers (VM, from left to right, *N,N*-dimethylacrylamide (DMA), 4-acryloylmorpholine (MORPH), *N*-isopropylacrylamide (NIPAM), and *N*-methoxypropylacrylamide (MPAM)) and multivinyl monomers (MVM, from left to right, *N,N*-methylene(bis)acrylamide (MBAM) and 1,4-bis(acryloyl)piperazine (PIPBAM)) used in this analysis. (C) Determination of the critical MVM concentration to reach gelation at full conversion ($[MVM]_{GP}$) using a growth boundary analysis. The R and Z termini arising from RAFT polymerizations bookend the primary chains. (D) Universal scaling behavior arising from knowledge of $[MVM]_{GP}$ affords molecular weight prediction.

the number and density of drugs or targeting ligands, affecting therapeutic function.[10]

While both step and chain-growth polymerization can be employed to synthesize polymeric networks, chain-growth mechanisms are often used due to the commercial availability of the building blocks and their synthetic ease. In this regard, the copolymerization of vinyl monomers (VM) and multivinyl monomers (MVM) yields polymer networks. However, the free-radical copolymerization of VMs and MVMs often suffers from poor control over network formation. Without the use of chain transfer agents (Strathclyde synthesis), it is nearly impossible to synthesize branched molecules without microscopic or macroscopic gelation.[38,39,41] Further, it is difficult to gain insight over both the average size of network's primary chains and M_x, resulting in convoluted network properties, which are difficult to predict.[40]

To address these limitations, polymer chemists have employed more sophisticated chain-growth methods to control synthetic network parameters. Self-condensing vinyl polymerization (SCVP) successfully avoids gelation; however, it lacks both control over the primary chains composing the branched networks and predictive power on the molecular weights of the synthesized networks.[42,43] Controlled radical polymerization (CRP) techniques, such as reversible addition fragmentation transfer (RAFT) or atom transfer radical polymerization (ATRP), yield low dispersities in primary chain lengths and successful postponement of macrosopic gelation.[44−47] Kinetic experiments employing degradable MVMs have demonstrated that primary chains in the CRP of VM and MVM grow in accordance with CRP kinetics and that branching occurs at high conversions.[48−52] Altering the ratio of [MVM]:[Chain Transfer Agent] ([CTA]) or [MVM]:[Initiator] allows topological control over the network structure from linear chains to branched networks to gels (Figure 1A).

Despite the synthetic ease and apparent modularity of the CRP-synthesized network polymers, it is not trivial to predict or model the network topology (M_x, M_n, and M_w) of these materials. While detailed kinetic studies have modeled the synthesis of network polymers and predicted both gel points and molecular radii as a function of conversion[53−55] and off lattice and dynamic lattice Monte Carlo simulations have been conducted to predict the gel point[56] and molecular weight scaling[57] of branched polymers in a network, they have not been explored for polymerizations under broad reaction conditions. The difficulty arising in these modeling approaches is largely driven by the variable ability of MVMs to form effective intermolecular cross-links or ineffective intramolecular loops. In this work, we explore experimental parameters that influence the cross-linking propensity of MVMs and work to quantitatively predict the resulting network structures by utilizing RAFT copolymerization of various VMs and MVMs (Figure 1B). We first develop a set of heuristics, derived from a Flory−Stockmayer analysis, to describe cross-link and loop forming behavior in the CRP of networks. We apply these heuristics within the growth boundary framework, developed by Wang and co-workers, to explore effects of both VM concentration and VM and MVM cross-propagation kinetics on cross-link efficiency (Figure 1C).[58−61] Through gel point normalization, we observe a universality in molecular weight scaling over broad reaction conditions (Figure 1D). Moreover, the normalization employed in this analysis reveals trends in the macroscopic mechanical properties of networks synthesized using CRP techniques. The gel point normalization technique developed in this manuscript allows the polymer chemist to target number and weight average molecular weights during the synthesis of (hyper)branched polymers using CRP. Simultaneously, the gel point normalization
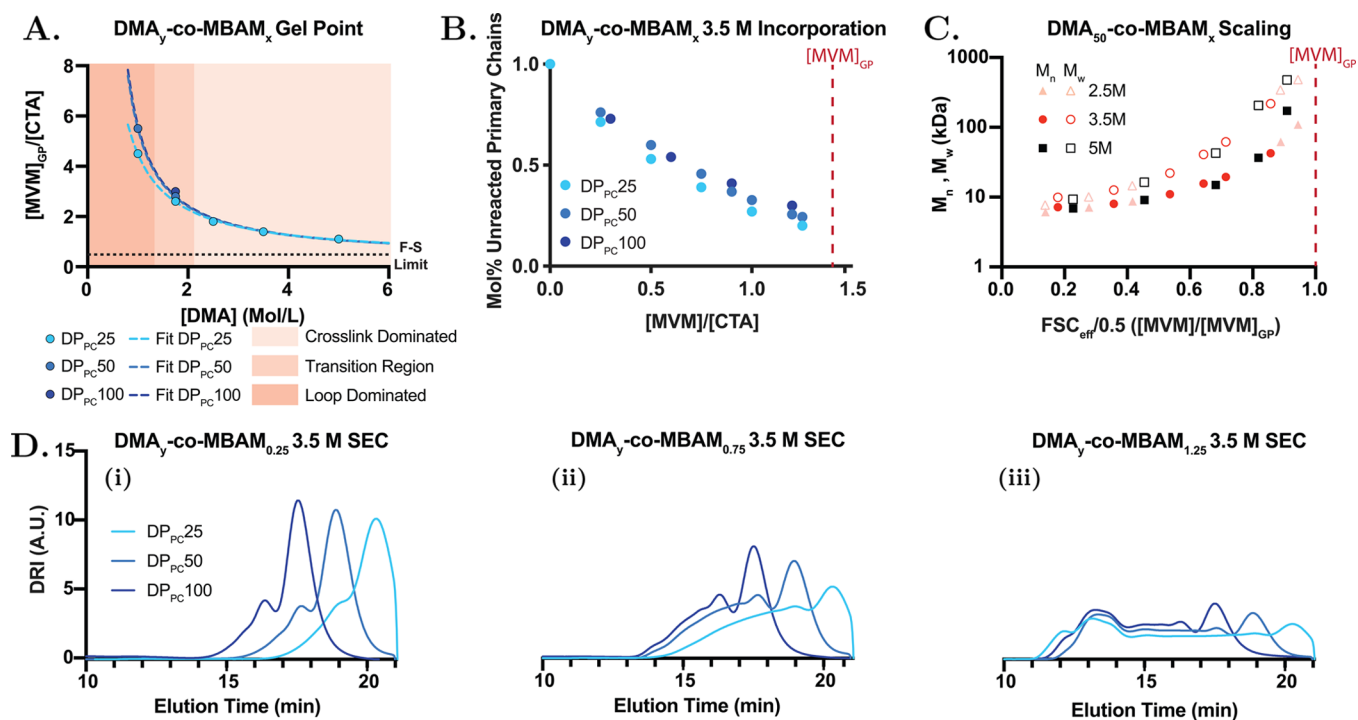
Figure 2. Study on network formation employing RAFT for the copolymerization of DMA and MBAM. (A) The critical $\frac{[MVM]_{GP}}{[CTA]}$ ratio at DP_{PC} 25 (light blue), 50 (blue), and 100 (dark blue) at [DMA] = 1, 1.75, 2.5, 3.5, and 5 M. The Flory–Stockmayer limit for gelation along with color coded regions describing intramolecular loop and intermolecular cross-link dominating regions are provided with a fit employing an effective molarity analysis for each DP_{PC} (regions are determined by the following criteria for $\frac{[MVM]_{GP}}{[CTA]}$: cross-link dominated <2 < transition Region <4 < loop dominated). (B) Molar fraction of unincorporated primary chains at distinct ratios of $\frac{[MVM]}{[CTA]}$ at fixed DP_{PC} of 25 (light blue), 50 (blue), and 100 (dark blue) at 3.5 M. The gel point from (A) (3.5 M) is depicted as a function of $\frac{[MVM]}{[CTA]}$. (C) Scaling of the number average (closed symbols) and weight average (open symbols) molecular weights of branched polymers plotted as a function of effective Flory–Stockmayer cross-links per primary chain (FSC_{eff}) in the cross-link-dominated zone. The gel point from (A) is depicted as a function of FSC_{eff}. (D) Size exclusion chromatograms (normalized by area under the curve) of the branched polymers at 3.5 M [DMA] at DP_{PC} 25 (light blue), 50 (blue), and 100 (dark blue) at $\frac{[MVM]}{[CTA]}$ ratios of (i) 0.25, (ii) 0.75, and (iii) 1.25 indicating incorporation of primary chains into the branched polymers.

technique demonstrates the utility of CRP techniques for the synthesis of covalent gels.

RESULTS AND DISCUSSION

Flory–Stockmayer Heuristics in Network Formation.
An understanding of how polymerization conditions lead to cross-link or loop formation is necessary to predict network topology. The Flory–Stockmayer model is often used to describe network formation in chain-growth systems, although it can be abstracted to network formation in CRP. In an idealized Flory–Stockmayer gelation model, each available functional moiety on a given monomer will react with its complementary moiety (cross-link formation) without the ability to self-terminate or cyclize (loop formation).[62] This model predicts macroscopic gelation at 100% conversion during the controlled copolymerization of VMs and MVMs at a 2:1 stoichiometry of primary chains to MVM ($\frac{[MVM]_{GP,ideal}}{[CTA]} = \frac{1}{2}$, $[MVM]_{GP}$ refers to the initial MVM concentration, which results in a gel point at 100% monomer conversion. The subscript ideal refers to a polymerization without loop formation).[53,63] We refer to this as the F–S ideality; however, loop formation necessitates higher concentration of MVM to reach gelation. We chose this criterion, as opposed to the experimentally observed limit of

$\frac{[MVM]_{GP,ideal}}{[CTA]} = 1$, due to the high percentage of loops observed in systems where $\frac{[MVM]_{GP}}{[CTA]} = 1$.[64] In this study, primary chains refer to the linear section of a CRP chain between the initiating moiety (in RAFT, the R terminal) and the living terminal (in RAFT, the Z terminal). To explore loop formation under broad reaction conditions, we develop a set of heuristics to describe effective cross-link and loop forming behaviors. The effective cross-link efficiency (XLE_{eff}), calculated using eq 1, describes the tendency of a MVM to form cross-links or loops for a given reaction condition. Moreover, the effective Flory–Stockmayer cross-links per primary chain (FSC_{eff}, eq 2) describe the stoichiometric distance from the gel point ($FSC_{eff,GP} = 0.5$). The purpose of the following section is to implement these heuristics in describing VM concentration effects on cross-link formation while demonstrating their utility in illustrating synthetic control over network formation in controlled radical polymerization.

$$XLE_{eff} = \frac{[CTA]}{2 \times [MVM]_{GP}} \tag{1}$$

$$FSC_{eff} = XLE_{eff} \times \frac{[MVM]}{[CTA]} \tag{2}$$

Seminal work by Armes, Matyjaszewski, and their respective co-workers illustrates that at a fixed primary chain degree of polymerization (DP_{PC}), XLE_{eff} is highly VM concentration dependent.[65,66] From a steric perspective, these studies demonstrate that primary chains below the overlap concentration ($c*$) tend toward intramolecular loop formation while primary chains above $c*$ favor intermolecular cross-linking. $c*$ calculations are provided in eq S1, which have been reported previously.[65,67] However, subsequent studies have indicated that the transition between the cross-link and loop-dominated concentration is not abrupt but gradual.[64]

To further probe the VM concentration dependence of macroscopic gelation, we copolymerize N,N-dimethylacrylamide (DMA) at fixed DMA molarities with N,N-methylene-(bis)acrylamide (MBAM) at DP_{PC} values of 25, 50, and 100 to full conversion. $[MVM]_{GP}$ was determined by varying MVM-to-CTA ratios for a given DP_{PC} until visible macroscopic gelation; the lowest MVM-to-CTA ratio that resulted in gelation was used to calculate $[MVM]_{GP}$. Macroscopic gelation is described as the resistance to flow upon vial inversion and the inability to dissolve upon addition of the polymerization solvent. The concentration dependence of $\frac{[MVM]_{GP}}{[CTA]}$ is plotted in Figure 2A, corroborating a gradual shift in XLE_{eff}. We hypothesize that the gradual shift is attributed to kinetic factors in network formation because interchain cross-linking is a bimolecular reaction while intrachain loop formation is a unimolecular reaction. To probe the interplay between the unimolecular and bimolecular kinetics of, respectively, loop and cross-link formation, we seek to fit the VM concentration dependence on $\frac{[MVM]_{GP}}{[CTA]}$ through an effective molarity analysis (EM, the ratio of the kinetic rate constant for loop formation to the kinetic rate constant for cross-link formation). We implement this to fit XLE_{eff} in eq 3, where $p*$ refers to the concentration of living radicals, approximated to the initiator concentration. We use the F−S condition for ideality and assume that each cross-link can either form a primary loop or cross-link. The experimental $\frac{[MVM]_{GP}}{[CTA]}$ values are converted into cross-link efficiencies to determine an effective molarity, as plotted in Figure S1. The effective molarities are between 10 and 200 μM, agreeing with previous literature values.[68] Moreover, for a given cross-link-to-primary chain ratio, $EM_{DP25} > EM_{DP50} > EM_{DP100}$. This agrees with the experimental observation of decreasing effective molarities with increasing distance between reactive species.[69−71] The calculated EM values are used to fit $\frac{[MVM]_{GP}}{[CTA]}$ in Figure 2A, which corroborate the unimolecular and bimolecular nature of loop and cross-link formation.

$$XLE_{eff} = \frac{1}{1 + \frac{[EM]^2}{[p*][MVM]}} \qquad (3)$$

Interestingly, varying DP_{PC} had little to no effect on $\frac{[MVM]_{GP}}{[CTA]}$. Because gelation is expected when $FSC_{eff} = 0.5$, these results imply that DP_{PC} does not affect XLE_{eff}. Moreover, because XLE_{eff} is unchanged, network formation or the buildup of primary chains into branched molecules remains unchanged. This is depicted in Figure 2B, where the molar fraction of unincorporated primary chains at regular intervals of $\frac{[MVM]}{[CTA]}$ is plotted at fixed DP_{PC} values of 25, 50, and 100 at 3.5 M ($p = $

0.27 to test the null hypothesis that the data sets share the same slope). As the cross-link-to-primary chain ratio is increased toward the critical ratio required for gelation, there is a regular and marked decrease in unincorporated primary chains until the gel point, which when extrapolated to the gel point, is not equal to 0. Representative SEC traces normalized by the area under the curve are presented in Figure 2D to illustrate this phenomenon. The primary chains in the SEC traces for DP_{PC} 25, 50, and 100 are the unresolved peaks at elution times of 20.5, 19, and 17.5 min, respectively.

When XLE_{eff} is unchanged, $\frac{[MVM]}{[CTA]}$ is a useful tool when comparing network formation between different polymerization conditions. However, when XLE_{eff} differs between samples, such as when [VM] concentration is altered, similarities in network formation arise when compared as a function of FSC_{eff}. The molecular weights of branched DP_{PC} 50 polymers synthesized at 2.5, 3.5, and 5 M, determined using size exclusion chromotography-multi angle laser light scattering (SEC-MALLS), are plotted in Figure 2C. The molecular weights for branched polymers synthesized at 3.5 M at DP_{PC} 25, 50, and 100 are presented in Figure S5. The number and weight average molecular weights are plotted as a function of $\frac{FSC_{eff}}{0.5}$, where a value of 1 represents the gel point. The similarity of the molecular weight scaling behavior demonstrates the utility of this analysis. XLE_{eff} is a unique descriptor for a polymerization environment. Moreover, it affords a stoichiometric normalization, FSC_{eff}, to demonstrate a similarity in network formation. It is important to note that at [VM] = 1 M, the branched synthesis of DMA and MBAM does not scale in this fashion. We presume that $\frac{[MVM]_{GP}}{[CTA]}$ is sufficiently large for the given DP_{PC} that steric and cooperative effects prevent $FSC_{eff} = XLE_{eff} \times \frac{[MVM]}{[CTA]}$. Thus, the following analysis in this manuscript occurs in the cross-link-dominated region ([VM] > 2.5 M).

In this section, we have developed heuristics to describe the complicated process of cross-link and loop formation during CRP of MVM and VM. We demonstrate that macroscopic gelation and network formation are a function of the number of effective cross-links on a primary chain (FSC_{eff}). We further show that FSC_{eff} is a function of the effective cross-link efficiency (XLE_{eff}) and dependent on VM concentration but independent of primary chain length (DP_{PC}). The VM concentration dependence of XLE_{eff} is fit via an effective molarity analysis, taking account of the, respective, unimolecular and bimolecular nature of loop and cross-link formation, reinforcing a gradual relationship between XLE_{eff} and [VM]. However, this analysis is limited to copolymerizations of DMA and MBAM. In the following section we explore a more nuanced understanding of the factors which affect XLE_{eff} through the copolymerization of different VM and MVMs.

Cross-Reactivity Kinetics Affect Effective Cross-link Efficiencies. To understand how VM and MVM selection affects XLE_{eff}, we draw from the kinetic growth boundary analysis developed by Wang and co-workers, which affords useful insight into the factors that direct a system to favor loop or cross-link formation.[58−61,72] The kinetic growth boundary can be visualized as the three-dimensional space a living radical occupies in its active state before becoming dormant; a graphical representation is provided in Figure 3A. For a given
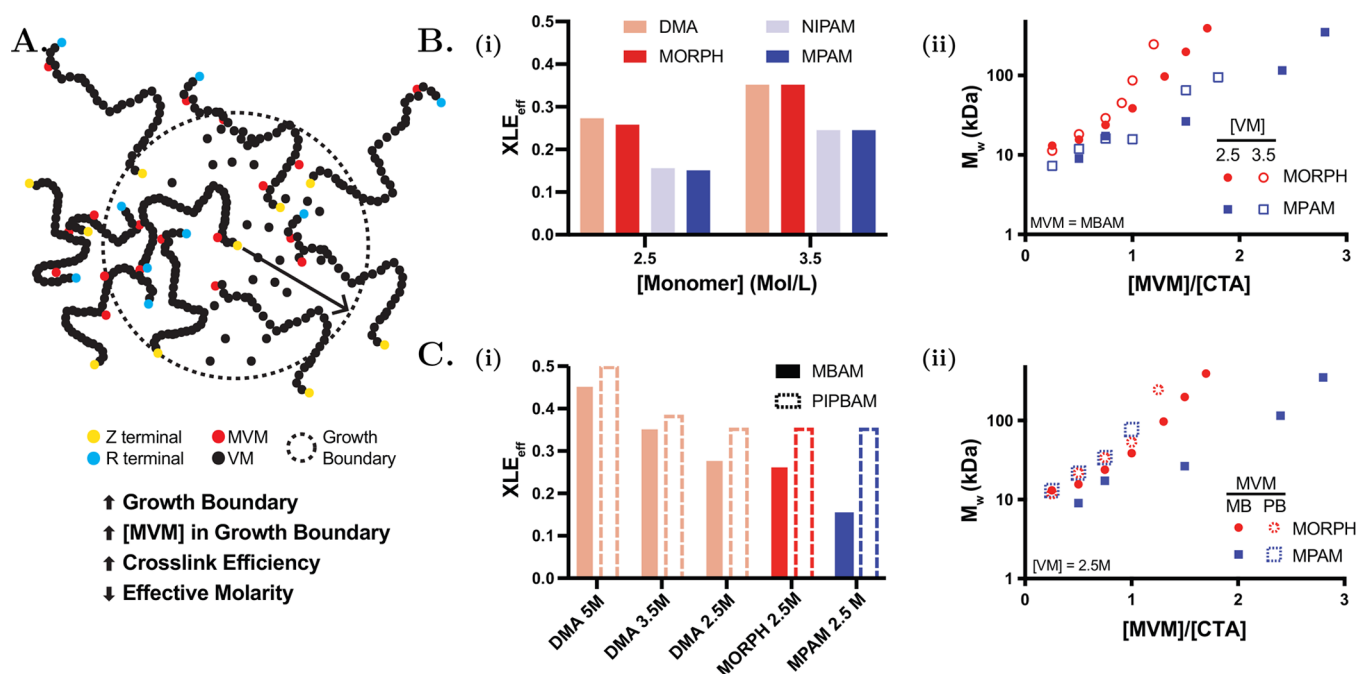
Figure 3. (A) Graphical representation of a growth boundary during RAFT polymerization. R and Z termini refer to the R and Z ends of the synthesized primary chains. The arrow is an illustrative tool indicative of the radius that a living radical can explore in its growth boundary. As more pendent MVMs enter the growth boundary through either increased concentration or growth boundary size, the effective cross-link efficiency (XLE$_{eff}$) increases. (B) (i) XLE$_{eff}$ and (ii) weight average molecular weight scaling behavior for MORPH (tertiary acrylamide) and MPAM (secondary acrylamide) at 2.5 and 3.5 M. (C) (i) XLE$_{eff}$ and (ii) weight average molecular weight scaling behavior for MORPH and MPAM at 2.5 M using MBAM (closed symbols) and PIPBAM (dashed symbols).

growth boundary, if the stoichiometric ratios of reactive groups remain constant, increasing the VM concentration will increase the number of polymer chains containing pendent vinyl groups inside the growth boundary, increasing XLE$_{eff}$. Similarly, for a given concentration and stoichiometric ratio of reactive groups, increasing the growth boundary's volume will increase the number of polymer chains in the growth boundary, increasing XLE$_{eff}$. Limiting the lifetime of the active sequence, effectively slowing polymerization kinetics, lowers XLE$_{eff}$.[59] We hypothesize that the cross-reactivity between the living radical and pendent vinyl unit is also a key factor for XLE$_{eff}$. Reducing the cross-reactivity kinetics of a living radical reacting with a pendent vinyl unit (increasing the reactivity ratio) increases the solution volume that a radical needs to sample before it reacts with a pendent vinyl chain, creating a larger effective growth boundary and a larger XLE$_{eff}$. In the following section, we aim to demonstrate the effects of cross-reactivity kinetics by (1) altering the reactivity and radical stability of the VM and (2) altering the steric availability of the MVM.

To adjust the reactivity and radical stability of the VM, we individually copolymerize four VMs (N,N-dimethylacrylamide (DMA), 4-acryloylmorpholine (MORPH), N-isopropylacrylamide (NIPAM), and N-methoxypropylacrylamide (MPAM)) with the MVM N,N-methylenebisacrylamide (MBAM) in the intermolecular cross-link-dominated region (2.5 and 3.5 M) at DP$_{PC}$ 50. These acrylamides are further classified into secondary (NIPAM and MPAM) and tertiary (DMA and MORPH) arylamides. The difference in resonance stabilization (Q) and polarity (e) of the radical on tertiary and secondary acrylamides, in accordance with Q-E formalism, results in nonrandom reactivity ratios for their copolymerization.[73] This was validated by measuring the reactivity ratios of NIPAM and DMA ($r_{N,2°} < r_{D,3°}$) and DMA and MORPH ($r_{D,3°} \approx r_{M,3°}$) in

Figure S4 using a nonlinear least-squares minimization of the integrated copolymer equation.[74,75] We plot XLE$_{eff}$ and M_w in Figure 3B-i,ii to probe the effects of VM radical stability.

Similar to the DMA EM analysis, XLE$_{eff}$ of each VM increases with molarity. Further, for a given molarity, the monomers in each acrylamide class (secondary or tertiary) contain identical XLE$_{eff}$. The XLE$_{eff}$ of the secondary acrylamides is smaller than those of tertiary acrylamides. The polymerization kinetics (k_p) at 3.5 M were measured for each monomer (Figure S2) and $k_{p,3°} < k_{p,2°}$, which are in accordance with growth boundary kinetic postulations. However, $k_{p,MORPH} < k_{p,DMA}$, yet XLE$_{MORPH} \approx$ XLE$_{DMA}$. This is likely because focusing on VM kinetics while ignoring cross-reactivity with the MVM affords an incomplete picture of the growth boundary. The increased reactivity ratios of tertiary acrylamides yield increased growth boundaries and XLE$_{eff}$s because they are statistically less likely to react with a pendent vinyl unit. Moreover, the reactivity ratio of the propagating VM is a dominant factor over polymerization kinetics in determining the growth boundary. Increased XLE$_{eff}$s lead to increasing slopes when M_w is plotted as a function of $\frac{[MVM]}{[CTA]}$. At a given molarity, MORPH (tertiary acrylamide) has a steeper slope than MPAM (secondary acrylamide). Further, both have steeper slopes at 3.5 M when compared to 2.5 M. $\frac{[MVM]}{[CTA]}$ is utilized here to reinforce how differences in XLE$_{eff}$ affect M_w scaling as a function of $\frac{[MVM]}{[CTA]}$ stoichiometry. However, when M_w is plotted as a function of FSC$_{eff}$, the M_ws scale identically (vide infra).

Many research groups have altered the XLE$_{eff}$ through altering the MVM.[49,76−79] Specifically, a study by Armes and co-workers demonstrates that a bulky MVM increases cross-
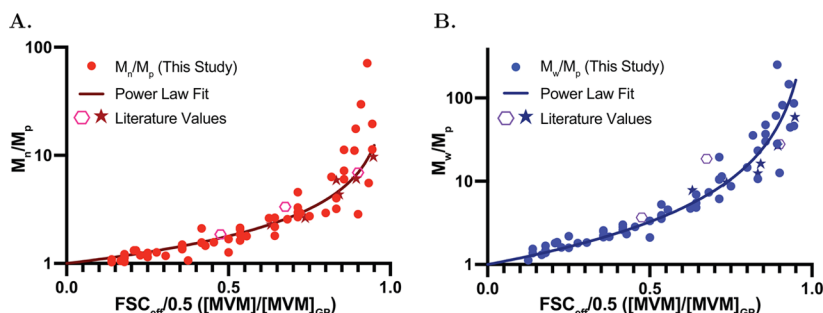
Figure 4. (A) Number average and (B) weight average primary chains per molecule determined by SEC-MALLS for polymerizations in the cross-link-dominated region ($[VM] \geq 2.5$ M) including literature polymerizations of acrylates using RAFT (hexagons)[49] and methacrylates using ATRP (stars).[65] A power law fit of our generated data (solid lines) is plotted with scaling exponents of 0.84 and 1.7 for the number and weight average primary chains per molecule, respectively.

linking efficiency.[49] From our cross-reactivity analysis, a bulky pendent MVM is sterically congested, increasing the reactivity ratio of the growing radical and increasing the XLE_{eff}. However, this provides no new insights regarding the hierarchy of electronic and steric effects on XLE_{eff}. We probe this hierarchy by copolymerizing 1,4-bis(acryloyl)piperazine (PIP-BAM) as the sterically hindered counterpart to MBAM. PIPBAM, however, is a tertiary acrylamide while MBAM is a secondary acrylamide. We copolymerize PIPBAM with DMA (2.5, 3.5, and 5 M), MPAM (2.5 M), and MORPH (2.5 M) to determine the XLE_{eff} (Figure 3C-i) and molecular weight scaling (Figure 3C-ii). Copolymerizations with PIPBAM, as compared to MBAM, yield higher XLE_{eff}, albeit PIPBAM has a smaller effect on XLE_{eff} when the XLE_{eff} with MBAM is sufficiently high.[78] This suggests that steric hindrance in the MVM imparts a large enough difference on the reactivity ratios to negate the effects from MVM Q and e values. In turn, sterics of the MVM are more important in determining XLE_{eff} than electronics. Moreover, for a given VM concentration (2.5 M), MORPH, MPAM, and DMA all had the same XLE_{eff} with PIPBAM despite having different XLE_{eff}s with MBAM. Similarly, MORPH and MPAM M_ws scale near identically when copolymerized with PIPBAM despite having different slopes when copolymerized with MBAM. This suggests that the involvement of steric hindrance in the MVM imparts a large enough difference on the reactivity ratios to negate the effects from VM Q and e values.

In this section, we introduced the nuance of cross-reactivity kinetics into the growth boundary analysis, illustrating its effects on XLE_{eff}. We test this hypothesis by polymerizing VMs with different kinetics but similar reactivity ratios and measure the resulting XLE_{eff}. We similarly adapt the effects of steric hindrance into a cross-reactivity kinetics argument and test this hypothesis by polymerizing VMs with a normal and sterically impaired MVM, demonstrating that the sterically impaired MVM increases the XLE_{eff}. Moreover, we reinforce the VM concentration effects of the previous section, demonstrating increased XLE_{eff} for each VM and MVM pair when the VM molarity is increased.

Universal Scaling Behavior in Network Polymers. We observe a universal scaling of molecular weights arising from the copolymerizations of VM and MVM when plotted as a function of FSC_{eff}. To illustrate this behavior, we plot the number and weight average primary chains per molecule. These values were determined by dividing M_n and M_w by M_p (peak molecular weight of the primary chain peak) for each polymerization in the cross-link-dominated region. These

values are plotted in Figure 4 and follow a power law relationship. A similar power law relationship is revealed when the data is plotted as a function of the relative extent of reaction (ϵ) in Figure S6. A table of all polymerization reactions implemented is provided in Table S4. We incorporate an ATRP copolymerization of methacrylates[65] and a RAFT copolymerization of acrylates[49] in this analysis. The use of ATRP for the branched copolymerization of methacrylates by Armes and co-workers shows good agreement for the 3 M and 5 M cases for M_n and M_w.[65] At first, it is surprising that their RAFT polymerizations from this same study do not fit this relationship (data not shown), given that the current analysis is derived from RAFT polymerization. However, the RAFT polymerizations of methacrylates were taken to approximately 95% conversion while their ATRP syntheses were taken to more than 99% conversion. It has been demonstrated that high molecular weight species evolve at high conversions. This was confirmed in a kinetic study that monitored the build up of high molecular weight species in a polymerization while maintaining traditional controlled growth of the primary chains (Figure S3). Because all pendent MVM groups have not reacted, it is unreasonable to expect the molecular weights in polymerizations at approximately 95% conversion to scale in a manner identical to copolymerizations that reached a full conversion. The RAFT copolymerization of acrylates by Armes and co-workers in a different study where $p \approx 1$ agrees with our findings.[49]

The experimental power law relationship is described in eq 4. The power law scaling exponents (γ) are measured as 0.84 and 1.7, respectively, for the number and weight average primary chains per branched copolymer molecule ($\frac{M_n}{M_p}$ and $\frac{M_w}{M_p}$). The universal power law relationship implies that once $[MVM]_{GP}$ is known for a VM and MVM pair (at a given VM concentration), a branched copolymer can be designed with specified $\frac{M_n}{M_p}$ and $\frac{M_w}{M_p}$.

$$\frac{M_{n,w}}{M_p} = \left(\frac{[MVM]_{GP}}{[MVM]_{GP}-[MVM]} \right)^{\gamma} \tag{4}$$

Network Formation beyond Gelation. The affine and phantom network theories dictate that the shear modulus (G') of a network scales linearly with $[MVM]$ ($G' \propto [MVM]$); however, recent synthetic and theoretical treatments have shown measurable deviation.[80−82] These deviations in the free-radical polymerization of VMs and MVMs arise from the

variable loop forming propensities and yield shear moduli that are difficult to predict a priori. However, Rosselgong and Armes have provided evidence that the measured XLE is independent of the MVM concentration.[64] Because of these observations, we hypothesize that the gel point normalization techniques employed in the previous section provide a functional analytical tool to study the macroscopic mechanical properties of covalent CRP gels.

We explore this hypothesis through the copolymerization of DMA and MBAM at two different DMA molarities (3.5 and 5 M) at a fixed DP_{PC}. The shear storage and loss modulus of the synthesized networks were determined by a frequency sweep test using an oscillatory shear rheometer. An example range of oscillatory storage modulus measurements for covalent networks of DMA (3.5 M) is presented in Figure S7. We determine full consumption of DMA by measuring the shear storage and loss moduli at cures of 24, 48, and 72 h (Figure S9) and with ^1H NMR spectroscopy (Figure S10). The shear storage moduli determined at 1 rad s^{-1} for each of the networks synthesized are presented in Figure 5. To employ gel
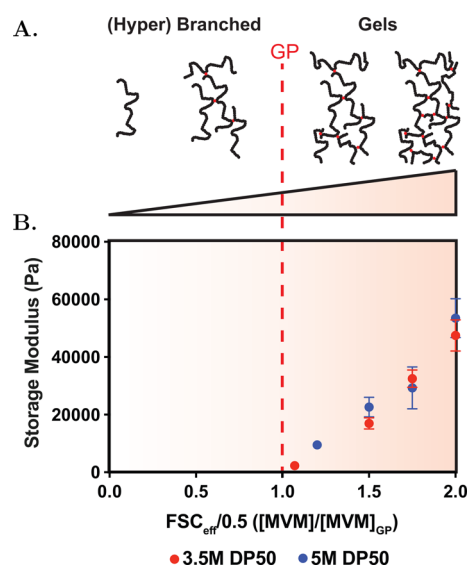
Figure 5. (A) Illustration of network formation comprising effective branch points (red dots) and primary chains (black chains) pre and post gelation. (B) Shear storage modulus (ω = 1 rad s^{-1}, ϵ = 0.01) of DMA gels polymerized at (1.2, 1.5, 1.75, and 2) $\times \frac{FSC_{eff}}{0.5}$ (5 M, DP_{PC} 50) and (1.1, 1.5, 1.75 and 2) $\times \frac{FSC_{eff}}{0.5}$ (3.5 M, DP_{PC} 50).

point normalization, the storage modulus is plotted as a function of both FSC_{eff} and $\frac{[MVM]}{[MVM]_{GP}}$. The shear storage modulus for each VM molarity appears to be linear, intersecting the x axis near the gel point. This is not necessarily surprising; branched polymers are often used as viscosity modifiers due to the inability of primary chains to entangle when the molecular weight between branch points is lower than the entanglement molecular weight (and monomer components display low associative character).[83] The expected elastic modulus of soluble networks should be orders of magnitude lower than that of the network post-gelation. The dynamic range of this analysis is limited to ranges of [MVM] where near full conversion of multivinyl monomers is still possible, and we hypothesize a plateau region for G' at higher [MVM] concentration.

It is surprising that we observe similar shear storage moduli for networks of DMA synthesized at 3.5 and 5 M. In the affine network model, the storage modulus is a function of entropic elasticity and derivative of the concentration of active strands and the molecular weight between cross-links. In this analysis, we assume that a cross-link can form either a primary loop or an effective cross-link. This approach predicts that at a fixed FSC_{eff}, the 3.5 and 5 M contain the same molecular weight between active cross-links yet different strand concentrations and the 5 M networks should have a larger storage modulus at a given FSC_{eff} than the 3.5 M network. However, this is not the case. While the formation of higher order loops is not detrimental to the prediction of $\frac{M_w}{M_p}$, the higher order loops maintain some degree of elasticity and affect the resulting mechanical properties of the network.[80−82] We do notice, however, that increasing DP_{PC} for a given [VM] and $\frac{[MVM]}{[MVM]_{GP}}$ lowers the shear storage modulus (Figure S8). The shear storage modulus for a 3.5 M DMA covalent gel $\left(\frac{[MVM]}{[MVM]_{GP}} = 2 \right)$ at DP_{PC} 100 is approximately 60% of the value of the shear storage modulus for DP_{PC} 50 at the same [VM] and normalized distance from the gel point. While the linear scaling of storage modulus when utilizing gel point normalization demonstrates the efficacy of this analysis, a full study that seeks to model and engineer these relationships requires future study.

■ CONCLUSIONS

Through gel point normalization, we describe a universality in the network formation of branched polymeric species using CRP. Specifically, knowledge of an experimental gel point for a VM and MVM combination at a given VM concentration allows the polymer chemist to predict the number and weight average molecular weight. Literature analysis of suitable data (accurate gel point determination and absolute molecular weight determination using light scattering) demonstrates the utility of this analysis for describing numerous distinct monomer classes and polymerization chemistries (e.g., ATRP and RAFT polymerization). The experimentally derived fitting parameter of this analysis, $[MVM]_{GP}$, has been explored as a function of reactivity ratios, kinetics, sterics, primary chain length, and concentration, providing useful insights regarding synthetic parameters. Last, through the realization of linear scaling trends, we demonstrate that gel point normalization is a promising tool to study the mechanical properties of CRP gels prepared through the copolymerization of VMs and MVMs.

■ EXPERIMENTAL SECTION

Materials. 2-Cyano-2-propyl dodecyl trithiocarbonate (2-CPDT, Strem, >97%), HPLC grade N,N-dimethylformamide (DMF, Alfa Aesar, >99.7%), CDCl$_3$ (Acros, >99.8%), and N,N′-methylenebis-(acrylamide) (MBAM, Sigma-Aldrich, 99%) were used as received. Vinyl monomers N,N-dimethylacrylamide (DMA, Sigma-Aldrich, 99%), N-(3-methoxypropyl)acrylamide (MPAM, Sigma-Aldrich, 95%), and 4-acryloylmorpholine (MORPH, TCI, >98%) were filtered with basic alumina before use. Vinyl monomer N-isopropylacrylamide (NIPAM, Acros, stabilized >99%) was recrystallized from hexanes (Fisher, certified ACS >99.9%) and dried under vacuum. MVM 1,4-diacrylylpiperazine (PIPBAM, CarboSynth, >98.5%) was dissolved in DMF and filtered with diatomaceous earth before use. 2,2′-Azobis(2-methylpropionitrile) (AIBN, Sigma, >98%) was recrystallized from

methanol (MeOH, Fisher, HPLC grade > 99.9%) and dried under vacuum before use.

Typical Synthesis of Branched Polymers. A typical procedure to synthesize a 5 M DMA-*co*-MBAM branched polymer targeting a MVM/CTA ratio of 1:1 and a VM/CTA ratio of 50 is as follows. Apart from VM and MVM selection and chosen molarity and DP_{PC}, the procedure is identical for other VM and MVM combinations. DMA (495 μg, 5 mmol, 50 equiv, filtered through basic alumina), MBAM (15.4 μg, 0.1 mmol, 1 equiv), 2-CPDT (34.6 μg, 0.1 mmol, 1 equiv), and AIBN (3.3 μg, 0.02 mmol, 0.2 equiv) were added to an 8 mL scintillation vial equipped with a PTFE septa and diluted to a final solution volume of 1 mL with DMF. The reaction mixture was sparged with nitrogen gas for 10 min and heated for 24 h at 60 °C. Monomer conversion was determined by ^{1}H NMR spectroscopy and the M_n and dispersity were obtained by SEC-MALLS.

Synthesis of Covalent Gels. A typical procedure to synthesize a 5 M DMA-*co*-MBAM covalent gel targeting a MVM/CTA ratio of 2.1:1 and a VM/CTA ratio of 50 is as follows. DMA (990 μg, 10 mmol, 50 equiv), MBAM (64.75 μg, 0.42 mmol, 2.1 equiv), 2-CPDT (69.2 μg, 0.2 mmol, 1 equiv), and AIBN (33 μg, 0.2 mmol, 1 equiv) were added to a 8 mL scintillation vial equipped with a PTFE septa and diluted to a final solution volume of 2 mL with DMF. The reaction mixture was sparged with nitrogen gas for 10 min. Two overlapping glass microscope slides (Fisherbrand, Superfrost Plus) separated by 1 mm PDMS (McMaster-Carr, High-Temperature Silicone Rubber Sheets) were fixed to a hot plate and covered with a Pyrex crystallizing dish wrapped with Parafilm to create a seal. The environment was heated to 60 °C and purged with nitrogen gas for 60 min. The reaction mixture was transferred with a purged syringe and injected between the two glass slides under the crystallization dish and heated at 60 °C for 24 h. A representation of the setup is depicted in Figure S11. The reaction was brought to room temperature and the glass slides were removed from the crystalization dish. Upon removal of a glass slide, rheology samples were prepared using a 10 mm biopsy punch (Robbins Instruments, True-Cut Disposable Biopsy Punch). Monomer conversion was determined by swelling a section of gel in CDCl$_3$ for 48 h before implementation of ^{1}H NMR spectroscopy.

Molecular Weight Determination Using Multi Angle Laser Light Scattering (THF). Absolute molecular weight and dispersity were determined in the ASTRA software package (Wyatt Technology Corporation) after passing through two size exclusion chromatography columns (Resolve 1000 Å DVB, ID 7.8 mm, M_w range 100−50,000 g mol^{-1} (Jordi Labs) and Resolve Mixed Bed Low DVB, ID 7.8 mm, M_w range 200−600,000 g mol^{-1} (Jordi Labs)) in a mobile phase tetrahydrofuran (THF) at 40 °C and a flow rate of 1.0 mL min^{-1}. Detection consisted of an Optilab T-rEX (Wyatt Technology Corporation) refractive index detector operating at 658 nm and a TREOS II light scattering detector (Wyatt Technology Corporation) operating at 659 nm. dn/dc values for MORPH, DMA, and MPAM (respectively 0.115, 0.11, and 0.096) were determined in THF in the ASTRA software package by batch injection of four samples of known concentrations into an Optilab T-rEX refractive index detector.

Molar Percentage of Unincorporated Primary Chains Using Size Exclusion Chromatography (DMF). SEC traces were determined after passing through two size exclusion chromatography columns (Resolve Mixed Bed Low DVB, ID 7.8 mm, M_w range 200−600,000 g mol^{-1} (Jordi Labs)) in a mobile phase of *N,N*-dimethylformamide (DMF) with 0.1 M LiBr at 35 °C and a flow rate of 1.0 mL min^{-1} (Dionex Ultimate 3000 pump, degasser, and autosampler (Thermo Fisher Scientific)). The molar percentage of unincorporated primary chains was determined using the differential refractive index output of the SEC traces. The area under the curve (AUC) of the primary chain (AUC_{PC}) was determined by measuring the AUC of the rightmost peak (primary chain) from the baseline to its apex (1/2 of the peak) and multiplying this value by 2. The molar percentage of unincorporated primary chains is calculated by dividing the AUC_{PC} by the AUC of the entire spectra.

Rheological Characterization. All rheometry experiments were performed on a torque-controlled Discover HR2 Rheometer (TA Instruments). Oscillatory frequency sweep measurements on materials

were performed using a 8 mm parallel plate geometry (Peltier plate steel) from 0.1 to 10 rad sec^{-1} at a strain (ϵ) of 0.01 at 20 °C maintaining an axial force of 0.03 N upon loading the sample.

■ ASSOCIATED CONTENT

Ⓢ Supporting Information

The Supporting Information is available free of charge at https://pubs.acs.org/doi/10.1021/acs.macromol.9b02109.

Effective molarity derivation and calculations; linear vinyl monomer kinetics; branched NIPAM-*co*-MBAM copolymerization kinetics; determination of reactivity ratios; molecular weights for branched copolymers synthesized in this study; alternative scaling analysis using ϵ, the extent of reaction; oscillatory sweep measurements, degree of cure measurements, and the experimental setup for CRP gel synthesis (PDF)

■ AUTHOR INFORMATION

Corresponding Author
*E-mail: eappel@stanford.edu.

ORCID Ⓘ
Eric A. Appel: 0000-0002-2301-7126

Notes
The authors declare no competing financial interest.

■ REFERENCES

(1) Weber, K.; Osborn, M. The Reliability of Molecular Weight Determinations by Dodecyl Sulfate-Polyacrylamide Gel Electrophoresis. *J. Biol. Chem.* **1969**, *244*, 4406−4412.

(2) Schägger, H.; von Jagow, G. Tricine-sodium dodecyl sulfate-polyacrylamide gel electrophoresis for the separation of proteins in the range from 1 to 100 kDa. *Anal. Biochem.* **1987**, *166*, 368−379.

(3) Shevchenko, A.; Wilm, M.; Vorm, O.; Mann, M. Mass Spectrometric Sequencing of Proteins from Silver-Stained Polyacrylamide Gels. *Anal. Chem.* **1996**, *68*, 850−858.

(4) Wichterle, O.; Lím, D. Hydrophilic Gels for Biological Use. *Nature* **1960**, *185*, 117−118.

(5) Musgrave, C. S. A.; Fang, F. Contact Lens Materials: A Materials Science Perspective. *Materials* **2019**, *12*, 261.

(6) Tse, J. R.; Engler, A. J. Preparation of Hydrogel Substrates with Tunable Mechanical Properties. *Curr. Protoc. Cell Biol.* **2010**, *47*, 10−16.

(7) Gao, X.; Zhang, X.; Wu, Z.; Zhang, X.; Wang, Z.; Li, C. Synthesis and physicochemical characterization of a novel amphiphilic polylactic acid-hyperbranched polyglycerol conjugate for protein delivery. *J. Controlled Release* **2009**, *140*, 141−147.

(8) Ye, L.; Letchford, K.; Heller, M.; Liggins, R.; Guan, D.; Kizhakkedathu, J. N.; Brooks, D. E.; Jackson, J. K.; Burt, H. M. Synthesis and Characterization of Carboxylic Acid Conjugated, Hydrophobically Derivatized, Hyperbranched Polyglycerols as Nanoparticulate Drug Carriers for Cisplatin. *Biomacromolecules* **2011**, *12*, 145−155.

(9) Wurm, F.; Dingels, C.; Frey, H.; Klok, H.-A. Squaric Acid Mediated Synthesis and Biological Activity of a Library of Linear and

Hyperbranched Poly(Glycerol-Protein Conjugates). *Biomacromolecules* **2012**, *13*, 1161−1171.

(10) Wang, D.; Zhao, T.; Zhu, X.; Yan, D.; Wang, W. Bioapplications of hyperbranched polymers. *Chem. Soc. Rev.* **2015**, *44*, 4023−4071.

(11) Saiyin, W.; Wang, D.; Li, L.; Zhu, L.; Liu, B.; Sheng, L.; Li, Y.; Zhu, B.; Mao, L.; Li, G.; Zhu, X. Sequential Release of Autophagy Inhibitor and Chemotherapeutic Drug with Polymeric Delivery System for Oral Squamous Cell Carcinoma Therapy. *Mol. Pharmaceutics* **2014**, *11*, 1662−1675.

(12) Yang, L.; Sun, H.; Liu, Y.; Hou, W.; Yang, Y.; Cai, R.; Cui, C.; Zhang, P.; Pan, X.; Li, X.; Li, L.; Sumerlin, B. S.; Tan, W. Self-Assembled Aptamer-Grafted Hyperbranched Polymer Nanocarrier for Targeted and Photoresponsive Drug Delivery. *Angew. Chem., Int. Ed.* **2018**, *57*, 17048−17052.

(13) Kim, K.; Lee, M.; Park, H.; Kim, J.-H.; Kim, S.; Chung, H.; Choi, K.; Kim, I.-S.; Seong, B. L.; Kwon, I. C. Cell-Permeable and Biocompatible Polymeric Nanoparticles for Apoptosis Imaging. *J. Am. Chem. Soc.* **2006**, *128*, 3490−3491.

(14) Sun, M.; Hong, C.-Y.; Pan, C.-Y. A Unique Aliphatic Tertiary Amine Chromophore: Fluorescence, Polymer Structure, and Application in Cell Imaging. *J. Am. Chem. Soc.* **2012**, *134*, 20581−20584.

(15) Boase, N. R. B.; Blakey, I.; Rolfe, B. E.; Mardon, K.; Thurecht, K. J. Synthesis of a multimodal molecular imaging probe based on a hyperbranched polymer architecture. *Polym. Chem.* **2014**, *5*, 4450−4458.

(16) Rolfe, B. E.; Blakey, I.; Squires, O.; Peng, H.; Boase, N. R. B.; Alexander, C.; Parsons, P. G.; Boyle, G. M.; Whittaker, A. K.; Thurecht, K. J. Multimodal Polymer Nanoparticles with Combined 19F Magnetic Resonance and Optical Detection for Tunable, Targeted, Multimodal Imaging in Vivo. *J. Am. Chem. Soc.* **2014**, *136*, 2413−2419.

(17) Wang, K.; Peng, H.; Thurecht, K. J.; Puttick, S.; Whittaker, A. K. Segmented Highly Branched Copolymers: Rationally Designed Macromolecules for Improved and Tunable 19F MRI. *Biomacromolecules* **2015**, *16*, 2827−2839.

(18) Hong, Y.; Cooper-White, J. J.; Mackay, M. E.; Hawker, C. J.; Malmström, E.; Rehnberg, N. A novel processing aid for polymer extrusion: Rheology and processing of polyethylene and hyperbranched polymer blends. *J. Rheol.* **1999**, *43*, 781−793.

(19) Hong, Y.; Coombs, S. J.; Cooper-White, J. J.; Mackay, M. E.; Hawker, C. J.; Malmström, E.; Rehnberg, N. Film blowing of linear low-density polyethylene blended with a novel hyperbranched polymer processing aid. *Polymer* **2000**, *41*, 7705−7713.

(20) Mulkern, T. J.; Tan, N. C. B. Processing and characterization of reactive polystyrene/hyperbranched polyester blends. *Polymer* **2000**, *41*, 3193−3203.

(21) Wang, J.; Ye, Z.; Zhu, S. Topology-Engineered Hyperbranched High-Molecular-Weight Polyethylenes as Lubricant Viscosity-Index Improvers of High Shear Stability. *Ind. Eng. Chem. Res.* **2007**, *46*, 1174−1178.

(22) Cicala, G.; Recca, G. Studies on epoxy blends modified with a hyperbranched polyester. *Polym. Eng. Sci.* **2008**, *48*, 2382−2388.

(23) Morgan, S.; Ye, Z.; Subramanian, R.; Zhu, S. Higher-molecular-weight hyperbranched polyethylenes containing crosslinking structures as lubricant viscosity-index improvers. *Polym. Eng. Sci.* **2010**, *50*, 911−918.

(24) Zheng, Y.; Thurecht, K. J.; Wang, W. Polysiloxanes polymers with hyperbranched structure and multivinyl functionality. *J. Polym. Sci. A* **2012**, *50*, 629−637.

(25) Hawker, C. J.; Chu, F.; Pomery, P. J.; Hill, D. J. T. Hyperbranched Poly(ethylene glycol)s: A New Class of Ion-Conducting Materials. *Macromolecules* **1996**, *29*, 3831−3838.

(26) Nishimoto, A.; Agehara, K.; Furuya, N.; Watanabe, T.; Watanabe, M. High Ionic Conductivity of Polyether-Based Network Polymer Electrolytes with Hyperbranched Side Chains. *Macromolecules* **1999**, *32*, 1541−1548.

(27) Lee, S.-I.; Schömer, M.; Peng, H.; Page, K. A.; Wilms, D.; Frey, H.; Soles, C. L.; Yoon, D. Y. Correlations between Ion Conductivity and Polymer Dynamics in Hyper-branched Poly(ethylene oxide) Electrolytes for Lithium-Ion Batteries. *Chem. Mater.* **2011**, *23*, 2685−2688.

(28) Fu, G.; Kyu, T. Effect of Side-Chain Branching on Enhancement of Ionic Conductivity and Capacity Retention of a Solid Copolymer Electrolyte Membrane. *Langmuir* **2017**, *33*, 13973−13981.

(29) Paranjape, N.; Mandadapu, P. C.; Wu, G.; Lin, H. Highly-branched cross-linked poly(ethylene oxide) with enhanced ionic conductivity. *Polymer* **2017**, *111*, 1−8.

(30) Peppas, N. A.; Reinhart, C. T. Solute diffusion in swollen membranes. Part I. A new theory. *J. Memb. Sci.* **1983**, *15*, 275−287.

(31) Amsden, B. Solute Diffusion within Hydrogels. Mechanisms and Models. *Macromolecules* **1998**, *31*, 8382−8395.

(32) am Ende, M. T.; Peppas, N. A. Transport of ionizable drugs and proteins in crosslinked poly(acrylic acid) and poly(acrylic acid-co-2-hydroxyethyl methacrylate) hydrogels. II. Diffusion and release studies. *J. Controlled Release* **1997**, *48*, 47−56.

(33) Engler, A. J.; Sen, S.; Sweeney, H. L.; Discher, D. E. Matrix Elasticity Directs Stem Cell Lineage Specification. *Cell* **2006**, *126*, 677−689.

(34) Huebsch, N.; Arany, P. R.; Mao, A. S.; Shvartsman, D.; Ali, O. A.; Bencherif, S. A.; Rivera-Feliciano, J.; Mooney, D. J. Harnessing traction-mediated manipulation of the cell/matrix interface to control stem-cell fate. *Nat. Mater.* **2010**, *9*, 518−526.

(35) Charrier, E. E.; Pogoda, K.; Wells, R. G.; Janmey, P. A. Control of cell morphology and differentiation by substrates with independently tunable elasticity and viscous dissipation. *Nat. Commun.* **2018**, *9*, 449.

(36) Burchard, W. Solution Properties of Branched Macromolecules. *Adv. Polym. Sci.* **1999**, *143*, 113−194.

(37) Yates, C. R.; Hayes, W. Synthesis and applications of hyperbranched polymers. *Eur. Polym. J.* **2004**, *40*, 1257−1281.

(38) Antonietti, M.; Rosenauer, C. Properties of fractal divinylbenzene microgels. *Macromolecules* **1991**, *24*, 3434−3442.

(39) O'Brien, N.; McKee, A.; Sherrington, D. C.; Slark, A. T.; Titterton, A. Facile, versatile and cost effective route to branched vinyl polymers. *Polymer* **2000**, *41*, 6027−6031.

(40) Denisin, A. K.; Pruitt, B. L. Tuning the Range of Polyacrylamide Gel Stiffness for Mechanobiology Applications. *ACS Appl. Mater. Interfaces* **2016**, *8*, 21893−21902.

(41) Costello, P. A.; Martin, I. K.; Slark, A. T.; Sherrington, D. C.; Titterton, A. Branched methacrylate copolymers from multifunctional monomers: chemical composition and physical architecture distributions. *Polymer* **2002**, *43*, 245−254.

(42) Hawker, C. J.; Frechet, J. M. J.; Grubbs, R. B.; Dao, J. Preparation of Hyperbranched and Star Polymers by a "Living", Self-Condensing Free Radical Polymerization. *J. Am. Chem. Soc.* **1995**, *117*, 10763−10764.

(43) Frechet, J. M.; Henmi, M.; Gitsov, I.; Aoshima, S.; Leduc, M. R.; Grubbs, R. B. Self-Condensing Vinyl Polymerization: An Approach to Dendritic Materials. *Science* **1995**, *269*, 1080−1083.

(44) Isaure, F.; Cormack, P. A. G.; Graham, S.; Sherrington, D. C.; Armes, S. P.; Bütün, V. Synthesis of branched poly(methyl methacrylate)s via controlled/living polymerisations exploiting ethylene glycol dimethacrylate as branching agent. *Chem. Commun.* **2004**, 1138−1139.

(45) Liu, B.; Kazlauciunas, A.; Guthrie, J. T.; Perrier, S. One-pot hyperbranched polymer synthesis mediated by reversible addition fragmentation chain transfer (RAFT) polymerization. *Macromolecules* **2005**, *38*, 2131−2136.

(46) Wang, A. R.; Zhu, S. Branching and gelation in atom transfer radical polymerization of methyl methacrylate and ethylene glycol dimethacrylate. *Polym. Eng. Sci.* **2005**, *45*, 720−727.

(47) Wang, A. R.; Zhu, S. Control of the polymer molecular weight in atom transfer radical polymerization with branching/crosslinking. *J. Polym. Sci. A* **2005**, *43*, 5710−5714.

(48) Li, Y.; Armes, S. P. Synthesis and Chemical Degradation of Branched Vinyl Polymers Prepared via ATRP: Use of a Cleavable Disulfide-Based Branching Agent. *Macromolecules* **2005**, *38*, 8155−8162.

(49) Vo, C. D.; Rosselgong, J.; Armes, S. P.; Billingham, N. C. RAFT synthesis of branched acrylic copolymers. *Macromolecules* **2007**, *40*, 7119−7125.

(50) Rosselgong, J.; Armes, S. P.; Barton, W.; Price, D. Synthesis of highly branched methacrylic copolymers: Observation of near-ideal behavior using RAFT polymerization. *Macromolecules* **2009**, *42*, 5919−5924.

(51) Pal, S.; Brooks, W. L. A.; Dobbins, D. J.; Sumerlin, B. S. Employing a Sugar-Derived Dimethacrylate to Evaluate Controlled Branch Growth during Polymerization with Multiolefinic Compounds. *Macromolecules* **2016**, *49*, 9396−9405.

(52) Liang, S.; Li, X.; Wang, W.-J.; Li, B.-G.; Zhu, S. Toward Understanding of Branching in RAFT Copolymerization of Methyl Methacrylate through a Cleavable Dimethacrylate. *Macromolecules* **2016**, *49*, 752−759.

(53) Wang, R.; Luo, Y.; Li, B.-G.; Zhu, S. Modeling of branching and gelation in RAFT copolymerization of vinyl/divinyl systems. *Macromolecules* **2009**, *42*, 85−94.

(54) Hernández-Ortiz, J. C.; Vivaldo-Lima, E.; Dubé, M. A.; Penlidis, A. Modeling of network formation in the atom transfer radical Co-polymerization (ATRP) of vinyl/divinyl monomers using a multifunctional polymer molecule approach. *Macromol. Theory Simul.* **2014**, *23*, 429−441.

(55) Hernández-Ortiz, J. C.; Vivaldo-Lima, E.; Dubé, M. A.; Penlidis, A. Modeling of network formation in reversible addition-fragmentation transfer (RAFT) copolymerization of vinyl/divinyl monomers using a multifunctional polymer molecule approach. *Macromol. Theory Simul.* **2014**, *23*, 147−169.

(56) Gao, H.; Polanowski, P.; Matyjaszewski, K. Gelation in living copolymerization of monomer and divinyl cross-linker: Comparison of ATRP experiments with Monte Carlo simulations. *Macromolecules* **2009**, *42*, 5925−5932.

(57) Bannister, I.; Billingham, N. C.; Armes, S. P. Monte Carlo modelling of living branching copolymerisation of monovinyl and divinyl monomers: Comparison of simulated and experimental data for ATRP copolymerisation of methacrylic monomers. *Soft Matter* **2009**, *5*, 3495−3504.

(58) Zheng, Y.; Cao, H.; Newland, B.; Dong, Y.; Pandit, A.; Wang, W. 3D single cyclized polymer chain structure from controlled polymerization of multi-vinyl monomers: Beyond flory-stockmayer theory. *J. Am. Chem. Soc.* **2011**, *133*, 13130−13137.

(59) Zhao, T.; Zheng, Y.; Poly, J.; Wang, W. Controlled multi-vinyl monomer homopolymerization through vinyl oligomer combination as a universal approach to hyperbranched architectures. *Nat. Commun.* **2013**, *4*, 1873.

(60) Gao, Y.; Zhou, D.; Zhao, T.; Wei, X.; McMahon, S.; O'Keeffe Ahern, J.; Wang, W.; Greiser, U.; Rodriguez, B. J.; Wang, W. Intramolecular Cyclization Dominating Homopolymerization of Multivinyl Monomers toward Single-Chain Cyclized/Knotted Polymeric Nanoparticles. *Macromolecules* **2015**, *48*, 6882−6889.

(61) Gao, Y.; Newland, B.; Zhou, D.; Matyjaszewski, K.; Wang, W. Controlled Polymerization of Multivinyl Monomers: Formation of Cyclized/Knotted Single-Chain Polymer Architectures. *Angew. Chem., Int. Ed.* **2017**, *56*, 450−460.

(62) Flory, P. J. Molecular Size Distribution in Three Dimensional Polymers. I. Gelation. *J. Am. Chem. Soc.* **1941**, *63*, 3083−3090.

(63) Gao, H.; Matyjaszewski, K. Synthesis of functional polymers with controlled architecture by CRP of monomers in the presence of cross-linkers: From stars to gels. *Prog. Polym. Sci.* **2009**, *34*, 317−350.

(64) Rosselgong, J.; Armes, S. P. Quantification of intramolecular cyclization in branched copolymers by 1H NMR spectroscopy. *Macromolecules* **2012**, *45*, 2731−2737.

(65) Rosselgong, J.; Armes, S. P.; Barton, W. R. S.; Price, D. Synthesis of branched methacrylic Copolymers: Comparison between

RAFT and ATRP and effect of varying the monomer concentration. *Macromolecules* **2010**, *43*, 2145−2156.

(66) Li, W.; Yoon, J. A.; Zhong, M.; Matyjaszewski, K. Atom transfer radical copolymerization of monomer and cross-linker under highly dilute conditions. *Macromolecules* **2011**, *44*, 3270−3275.

(67) Li, Y.; Ryan, A. J.; Armes, S. P. Synthesis of Well-Defined Branched Copolymers by Quaternization of Near-Monodisperse Homopolymers. *Macromolecules* **2008**, *41*, 5577−5581.

(68) Motloch, P.; Hunter, C. A. *Advances in Physical Organic Chemistry*; Academic Press: Cambridge, MA, 2016; Vol. *50*, pp 77−118.

(69) Krishnamurthy, V. M.; Semetey, V.; Bracher, P. J.; Shen, N.; Whitesides, G. M. Dependence of effective molarity on linker length for an intramolecular protein-ligand system. *J. Am. Chem. Soc.* **2007**, *129*, 1312−1320.

(70) Cacciapaglia, R.; Di Stefano, S.; Mandolini, L. Effective Molarities in Supramolecular Catalysis of Two-Substrate Reactions. *Acc. Chem. Res.* **2004**, *37*, 113−122.

(71) Misuraca, M. C.; Grecu, T.; Freixa, Z.; Garavini, V.; Hunter, C. A.; Van Leeuwen, P. W. N. M.; Segarra-Maset, M. D.; Turega, S. M. Relationship between conformational flexibility and chelate cooperativity. *J. Org. Chem.* **2011**, *76*, 2723−2732.

(72) Zheng, Y.; Newland, B.; Tai, H.; Pandit, A.; Wang, W. Single cyclized molecule structures from RAFT homopolymerization of multi-vinyl monomers. *Chem. Commun.* **2012**, *48*, 3085−3087.

(73) Alfrey, T.; Price, C. C. Relative reactivities in vinyl copolymerization. *J. Polym. Sci.* **1946**, *2*, 101−106.

(74) Meyer, V. E.; Lowry, G. G. Integral and differential binary copolymerization equations. *J. Polym. Sci. A* **1965**, *3*, 2843−2851.

(75) Van Den Brink, M.; Van Herk, A. M.; German, A. L. Nonlinear regression by visualization of the sum of residual space applied to the integrated copolymerization equation with errors in all variables. I. Introduction of the model, simulations and design of experiments. *J. Polym. Sci. A* **1999**, *37*, 3804−3816.

(76) Huang, W.; Yang, H.; Xue, X.; Jiang, B.; Chen, J.; Yang, Y.; Pu, H.; Liu, Y.; Zhang, D.; Kong, L.; Zhai, G. Polymerization behaviors and polymer branching structures in ATRP of monovinyl and divinyl monomers. *Polym. Chem.* **2013**, *4*, 3204−3211.

(77) Xue, X.; Wang, Y.; Huang, W.; Yang, H.; Chen, J.; Fang, J.; Yang, Y.; Kong, L.; Jiang, B. New insight into the ATRP of monovinyl and divinyl monomers. *Macromol. Chem. Phys.* **2015**, *216*, 1555−1561.

(78) Gao, H.; Li, W.; Matyjaszewski, K. Synthesis of polyacrylate networks by ATRP: Parameters influencing experimental gel points. *Macromolecules* **2008**, *41*, 2335−2340.

(79) Gao, H.; Miasnikova, A.; Matyjaszewski, K. Effect of cross-linker reactivity on experimental gel points during ATRcP of monomer and cross-linker. *Macromolecules* **2008**, *41*, 7843−7849.

(80) Zhong, M.; Wang, R.; Kawamoto, K.; Olsen, B. D.; Johnson, J. A. Quantifying the impact of molecular defects on polymer network elasticity. *Science* **2016**, *353*, 1264−1268.

(81) Chan, D.; Ding, Y.; Dauskardt, R. H.; Appel, E. A. Engineering the Mechanical Properties of Polymer Networks with Precise Doping of Primary Defects. *ACS Appl. Mater. Interfaces* **2017**, *9*, 42217−42224.

(82) Wang, J.; Lin, T.-S.; Gu, Y.; Wang, R.; Olsen, B. D.; Johnson, J. A. Counting Secondary Loops Is Required for Accurate Prediction of End-Linked Polymer Network Elasticity. *ACS Macro Lett.* **2018**, *7*, 244−249.

(83) Schubert, C.; Osterwinter, C.; Tonhauser, C.; Schömer, M.; Wilms, D.; Frey, H.; Friedrich, C. Can hyperbranched polymers entangle? Effect of hydrogen bonding on entanglement transition and thermorheological properties of hyperbranched polyglycerol melts. *Macromolecules* **2016**, *49*, 8722−8737.